Effect of weak solute advection on a chemically active particle under the influence of an external concentration gradient

Prathmesh M. Vinze and S. Pushpavanam*
Department of Chemical Engineering, Indian Institute of Technology Madras, Chennai, Tamil Nadu 600036, India

(Received 18 August 2021; accepted 4 November 2021; published 2 December 2021)

Janus particles are a class of artificial swimmers with an anisotropic coverage of catalyst on its surface. This generates a tangential chemical gradient. Solute molecules interact with the particle surface via a short-range potential. The asymmetric distribution of solute molecules gives rise to a tangential pressure gradient near the particle surface. This results in diffusio-osmotic flows in a thin region at the particle surface. The flow inside the thin layer is modeled as an effective slip velocity at the particle scale. This slip results in self-propulsion of a freely suspended particle, even in the absence of externally imposed concentration gradients. Previous studies have shown significant similarity between artificial and biological chemotaxis. Based on the magnitude of Péclet number (ratio of advective to diffusive effects), advective effects can have a moderate effect on the swimming velocity of an artificial swimmer. The current work aims at developing a theoretical framework to capture weak advective effects on the swimming velocity of an active particle under the influence of an external concentration gradient. It can be applied for any active particle with an axisymmetric surface activity distribution. Using Péclet number as a perturbation parameter, we employ a singular perturbation technique along with the method of matched assymptotic expansions to evaluate the concentration field up to $O(\mathrm{Pe})$. Using the Lorentz reciprocal theorem, an analytical expression for the translational velocity valid up to $O(\mathrm{Pe})$ is obtained. We show $O(\mathrm{Pe})$ correction of solute advection always reduces the swimming velocity.

DOI: 10.1103/PhysRevFluids.6.124201

I. INTRODUCTION

Over the recent past there has been a significant increase in research on self-propulsion of microparticles. These particles convert the chemical energy present in the environment into the mechanical energy needed for their self-propulsion. The swimming motion is characterized by low Reynolds number ($\mathrm{Re} \sim 10^{-6}$), which requires a break in fore aft symmetry [1]. For a microorganism, this is achieved through cellular appendages i.e., flagella or cilia present on its surface. These actuate in a wavelike motion on the surface to "push" or "pull" the microorganism, thereby achieving self-propulsion [2,3].

On the other hand, artificial swimmers typically self-propel via asymmetry in the surface properties [4–6] (such as surface activity, surface mobility, surface absorbance, etc.). For instance, a Janus particle coated asymmetrically with a catalyst can generate a near surface tangential chemical gradient. This generates the necessary tangential potential energy gradient for self-propulsion. The study of artificial swimmers has gained a renewed interest due to its potential application in drug delivery.

*spush@iitm.ac.in

Microorganisms typically exhibit chemotaxis, i.e., they respond to chemical gradients present in the environment. Specifically, *E.coli* moves towards a nutrient-rich region and is repelled from toxic environments by sensing the local concentration gradient and accordingly regulating its complex flagellar rotations [7–9]. Chemical signals sent out by mammalian eggs also help sperm cells to navigate and move towards the eggs [10,11]. Recent works have shown significant similarity between biological and artificial chemotaxis [12,13]. Artificial swimmers have been shown to "seek" an external concentration gradient.

Derjaguin and coworkers [14] were the first to study diffusiophoresis, i.e., movement of colloidal particles in concentration gradients. Later, Anderson [15] mathematically modeled the diffusiophoresis of an inert particle using a continuum framework. They showed that the external gradient creates an asymmetric interaction (attraction or repulsion) inside a thin layer around the particle, which creates a pressure gradient. The pressure gradient drives the fluid inside a thin layer, causing diffusio-osmosis. Fluid flow inside the thin layer is represented as a slip velocity at the particle scale, leading to the motion of the particle. The model at the particle scale considers diffusion as the dominant mechanism for transport of solute molecules.

Self-diffusiophoresis is another such mechanism, which results in self-propulsion of micron to sub-micron-sized particles. Howse *et al.* [5] synthesized a particle with platinum coated on one half and a nonconducting polystyrene on the other. The particles were placed in a solution with hydrogen peroxide. The peroxide reacts on the platinum-coated surface and creates a local concentration gradient inducing near surface flows, resulting in self-propulsion of particles. Golestanian *et al.* [18] developed a theoretical model of self-propelling Janus particles in a continuum framework. The mathematical model is based on three primary assumptions: (1) the interactive layer is thin compared to the size of the particle, allowing the fluid flow inside the thin layer to be approximated as a slip velocity at the surface, (2) diffusion was the dominant mode of solute transport, and (3) a fixed rate of adsorption or desorption of solute capture or release occurred at the "active" site. They concluded that an asymmetric surface activity is necessary for the self-propulsion of a chemically active particle. Micron-sized particles propelling using self-generated gradient of electric potential have also been synthesized recently [4,16,17]. This mechanism is termed as "self-electrophoresis."

Michelin and Lauga [19] applied numerical methods to explore solute advection and reactive effects on the swimming velocity of a Janus particle placed in a solution of uniform solute concentration. The calculations were made for a (i) half-face Janus particle and (ii) nonsymmetric Janus particle. The effect of Péclet number was found to be significant only for $\mathrm{Pe} > O(1)$ for both the particles.

More recently, Natale *et al.* [20] investigated the effect of solute advection on the swimming velocity of a Janus sphere in a weakly viscoelastic medium. They used a combination of perturbation and numerical methods. The governing equations were perturbed for small Deborah numbers (ratio of relaxation timescale to the characteristic timescale), and the advection diffusion equation was solved numerically at each order. Large local viscoelastic stresses were observed due to discontinuity in the surface activity. Solute advection sharpens or reduces the local concentration gradient, thus directly enhancing or diminishing the viscoelastic stresses. A significant effect of solute advection was seen for $\mathrm{Pe} > O(1)$.

Using perturbation expansion in Pe, Keh and Weng [21] investigated the effect of solute advection on the swimming velocity of a neutral particle placed in an external concentration gradient. The method of matched asymptotic expansions was employed to evaluate the $O(\mathrm{Pe}^2)$ correction to the swimming velocity. The formulation employed is similar to that used for thermophoretic spheres or bubbles by Subramanian [22] and Leshansky *et al.* [23]. However, the physical origin of thermophoresis is gradient in Marangoni stress.

Recently, Khair [24] extended Keh and Weng's work to account for two particle interactions. The formulation employed matched asymptotic expansion to evaluate the effect of advection for small but finite Péclet number. Numerical methods were employed to investigate the effect of solute advection for larger Péclet number. It was found that the solute advection reduced the strength of concentration gradient locally, causing a decrease in translational velocity with increase in Péclet

number. For a nonspherical particle, the translational velocity was found to be dependent on the shape and orientation .

Popescu *et al.* [25] qualitatively investigated artificial chemotaxis and showed that an additional symmetry breaking in surface mobility is required for the artificial swimmer to "sense" the external gradient. Tatulea-Codrean and Lauga [26] theoretically studied artificial chemotaxis of a Janus particle. The reaction at the active surface followed Michaelis-Menten kinetics in the limit of low substrate concentration. In this limit the reaction rate becomes proportional to the substrate concentration. Here, both substrate and the product interact with the particle, leading to chemotaxis. The same problem in the limit of high substrate (solute) concentration was studied by Vinze *et al.* [27].

Typically, Péclet number associated with artificial swimmers is of the order 10^{-2}. This suggests, solute advection can play a modest role in artificial chemotactic systems. Thus, quantifying its effect will help in designing potential drug delivery applications. To obtain insights into the role of solute advection, we theoretically investigate the effect on the translation of an active particle in a linear concentration gradient to $O(\mathrm{Pe})$. The mathematical formulation of the problem is presented in Sec. II. Here we describe the characteristic scales present in the system and render the equations dimensionless. We perturb the system for a small but finite value of Péclet number. We investigate the effect of solute advection after the particle has reoriented. This results in an axisymmetric system. In Sec. III, using the principle of linearity and superposition, we first solve for the concentration field at the leading order. The velocity field is then solved using a stream-function formulation, and the singular nature of this problem is identified. In Sec. IV, due to the singular nature, we divide the domain into two regions and solve in each region separately and match them using Van Dyke's principle [28]. Using the Lorentz reciprocal theorem, the swimming velocity corrected up to $O(\mathrm{Pe})$ is obtained in Sec. V. We analyze the system for different surface coverages of the activity and report the corrected velocity expression valid up to $O(\mathrm{Pe})$. Lastly, in Sec. VI we conclude with the physical insights obtained from this study and present future perspectives.

II. PROBLEM FORMULATION

Consider a chemically active particle of radius a^* under the influence of an external linear concentration gradient of strength (γ^*). The superscript * denotes a dimensional quantity. The surface activity of the particle is taken to be axisymmetric and a smooth function of the polar angle [$\alpha^*(\theta)$]. The surface activity characterizes the rate of adsorption or desorption of solute molecules on the surface of the particle. The interaction of the solute molecules with the particle surface is characterized by a mobility coefficient μ^*. Repulsive interactions lead to a positive value of μ^*, and vice versa. The main aim of this study is to quantify the effect of solute advection on the swimming velocity of a chemically active particle. The current study quantifies the role of solute advection after the particle has reoriented along the external concentration gradient. The external concentration is along the axis of symmetry of the active particle as shown in Fig. 1. The external concentration field is given by

$$C^*_\infty = \gamma^* z'^*. \tag{1}$$

The imposed concentration gradient is in a stationary frame of reference. It is transformed in the moving frame using

$$z'^* = z^* + U^*_s t^*. \tag{2}$$

Here U^*_s is the swimming velocity of the particle. Substituting Eq. (2) into (1), the imposed concentration field is given by

$$C^*_\infty = \gamma^*(z^* + U^*_s t^*). \tag{3}$$

The characteristic length scale in the system is $l_{ch} = a^*$. Velocity scale is taken as a sum of the characteristic scales arising from surface activity and the external concentration gradient,

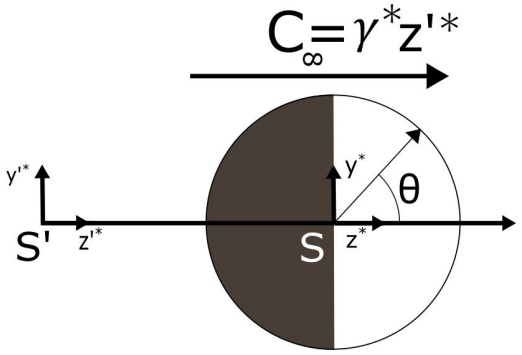

FIG. 1. Schematic depicting the two frames of references. S' is the rest frame of reference while S denotes the moving frame of reference. The system is axisymmetric with external concentration gradient C_∞ along the axis of symmetry. Gray and white colors represent different surface activity.

$u_{ch} = \mu^*(\gamma^* + \frac{\alpha^*}{D^*})$. Here, α^* represents the maximum magnitude of the surface activity. The timescale is taken as $t_{ch} = \frac{l_{ch}}{u_{ch}}$ and the characteristic concentration as $C_{ch} = \frac{\alpha^* a^*}{D^*}$, where D^* is the diffusion coefficient of solute molecules in the fluid. The pressure characteristic scale is $P_{ch} = \frac{\nu^* u_{ch}}{l_{ch}}$. A dimensionless number ($A = \frac{\gamma^* D^*}{\alpha^*}$) is introduced which expresses the relative strength of the external gradient compared to the self-generated gradient. Using the above characteristic scales, the dimensionless solute and momentum balance in the particle (moving frame of reference) frame is given as

Solute balance:

$$\mathrm{Pe}\left(\frac{\partial c}{\partial t} + \mathbf{u}\cdot\nabla c\right) = \nabla^2 c, \tag{4}$$

$$c \to C_\infty \quad \text{as} \quad r \to \infty, \tag{5}$$

$$-\mathbf{n}\cdot\nabla c = \alpha(\theta) \quad \text{at} \quad r = 1. \tag{6}$$

Momentum balance:

$$\mathrm{Re}\left(\frac{\partial \mathbf{u}}{\partial t} + \mathbf{u}\cdot\nabla\mathbf{u}\right) = -\nabla P + \nabla^2\mathbf{u}, \tag{7}$$

$$\mathbf{u} \to -\mathbf{U_s} \quad \text{as} \quad r \to \infty, \tag{8}$$

$$\mathbf{u} = \frac{\mu(\mathbf{I} - \mathbf{nn})\cdot\nabla c}{A+1} \quad \text{at} \quad r = 1. \tag{9}$$

Here the far field concentration field $C_\infty = A(r\cos\theta + U_s t)$. Equations (4)–(9) completely govern the dynamics of solute and momentum transport. The concentration field is coupled with the velocity field via the slip velocity relation given by (9). Two dimensionless numbers describing the system behavior are $\mathrm{Pe} = \frac{u^*_{ch} a^*}{D^*}$ and $\mathrm{Re} = \frac{u^*_{ch} a^*}{\nu^*}$. For a particle of size 10 μm, with swimming velocity of order $\sim$1 μm/s, taking the diffusion coefficient as 2.3×10^{-9} m^2/s and kinematic viscosity of water as $1.05\times10^{-6}\,\mathrm{m}^2/\mathrm{s}$, the Reynolds number and Péclet number are 9.52×10^{-6} and 4.3×10^{-2}, respectively. The Reynolds number suggests that fluid advection plays a negligible role. Therefore the assumption of Stokes flow is reasonable for such problems. However, the Péclet number suggests weak or moderate solute advection exists. To quantify this effect and obtain physical insights, in this work we use a perturbation technique to find the effect of solute convection to first order in Pe. We

seek a solution of the form

$$\begin{aligned} c &= c_0(r,t) + \mathrm{Pe}c_1(r,t) + O(\mathrm{Pe}^2) \\ \mathbf{u} &= \mathbf{u}_0(r,t) + \mathrm{Pe}\mathbf{u}_1(r,t) + O(\mathrm{Pe}^2) \\ P &= P_0(r,t) + \mathrm{Pe}P_1(r,t) + O(\mathrm{Pe}^2). \end{aligned} \tag{10}$$

This leads to the slip velocity and the swimming velocity of the form

$$\begin{aligned} \mathbf{u_{slip}} &= \mathbf{u_{slip},0} + \mathrm{Pe}\mathbf{u_{slip},1} + O(\mathrm{Pe}^2) \\ \mathbf{U_s} &= \mathbf{U_{s,0}} + \mathrm{Pe}\mathbf{U_{s,1}} + O(\mathrm{Pe}^2), \end{aligned} \tag{11}$$

where $\boldsymbol{u}_{\mathrm{slip},0}$ and $\boldsymbol{U}_{s,0}$ are the contribution of the slip velocity at the leading order (without solute convection), while $\boldsymbol{u}_{\mathrm{slip},1}$ and $\boldsymbol{U}_{s,1}$ account for the first order advective effects on the slip velocity and swimming velocity. Substituting Eq. (10) into Eqs. (4)–(9), we obtain the governing equations at each order of Péclet number. At leading order we obtain

Solute transport:

$$\nabla^2 c_0 = 0, \tag{12}$$

$$-\mathbf{n}\cdot\nabla c_0 = \alpha(\theta) \quad \text{at } r = 1, \tag{13}$$

$$c_0 \to C_\infty \quad \text{as r} \to \infty \tag{14}$$

Momentum transport:

$$\nabla^2 \mathbf{u}_0 - \nabla P_0 = 0, \tag{15}$$

$$\mathbf{u}_0 = -\mathbf{U}_{s,0} \quad \text{as } r \to \infty, \tag{16}$$

$$\mathbf{u}_0 = \frac{\mu(\mathbf{I}-\mathbf{nn})\cdot\nabla c_0}{A+1} \quad \text{at r} = 1. \tag{17}$$

At $O(\mathrm{Pe})$ we have

Solute transport:

$$\nabla^2 c_1 = \frac{\partial c_0}{\partial t} + \mathbf{u}_0\cdot\nabla c_0, \tag{18}$$

$$-\mathbf{n}\cdot\nabla c_1 = 0 \quad \text{at } r\text{= } 1, \tag{19}$$

$$c_1 \to 0 \quad \text{as } r \to \infty. \tag{20}$$

Momentum transport:

$$\nabla^2 \mathbf{u}_1 - \nabla P_1 = 0, \tag{21}$$

$$\mathbf{u}_1 = -\mathbf{U}_{s,1} \quad \text{as } r \to \infty, \tag{22}$$

$$\mathbf{u}_1 = \frac{\mu(\mathbf{I}-\mathbf{nn})\cdot\nabla c_1}{A+1} \quad \text{at } r = 1. \tag{23}$$

The advective effects of the solute do not contribute at the leading order. The correction to the swimming velocity due to advection is realized at $O(\mathrm{Pe})$. The solute advection appears as a source term at $O(\mathrm{Pe})$ in (18). Following previous studies [21,22,24], we describe the solution procedure for the above equations at each order, starting from the leading order in the next section.

III. SOLUTION OF CONCENTRATION AND VELOCITY FIELD AT LEADING ORDER

A. Concentration field

The concentration field is governed by Eqs. (12)–(14) at O(Pe^0). Following previous works of Subramanian [22] and Khair [24], we define a steady disturbance field $c_0'(r) = c_0(r,t) - C_\infty(r,t)$. This is governed by

$$\nabla^2 c_0' = 0, \tag{24}$$

$$-\mathbf{n}\cdot\nabla c_0' = \alpha(\theta) + A\cos\theta, \tag{25}$$

$$c_0' \to 0. \tag{26}$$

Following [27], the solution to (24)–(26) is given by

$$c_0' = \frac{A\eta}{2r^2} + \sum_{l=0}^{\infty} \frac{\alpha_l r^{-(l+1)}}{l+1} P_l(\eta), \tag{27}$$

where $\eta = \cos\theta$, $P_l(\eta)$ is the Legendre polynomial of order l and α_l is the lth spectral mode of surface activity distribution. The first term arises from the contribution of external concentration gradient while the second term appears due to surface activity. The leading order disturbance in (27) decays as O$(1/r)$, which corresponds to $\mathrm{l} = 0$ mode of surface activity. The concentration field at leading order is given by $c_0(r,t) = c_0'(r) + C_\infty(r,t)$:

$$c_0 = Ar\eta + AU_{s,0}t + \frac{A\eta}{2r^2} + \sum_{l=0}^{\infty} \frac{\alpha_l r^{-(l+1)}}{l+1} P_l(\eta). \tag{28}$$

B. Velocity field

The velocity field is governed by (15)–(17), where $\boldsymbol{U}_{s,0}$ is the leading order swimming velocity of the particle. Using (28), the slip velocity at the surface is evaluated as

$$\mathbf{u_{slip,0}} = \frac{-\mu\sqrt{1-\eta^2}}{A+1}\left(\frac{3A}{2} + \sum_{l=0}^{\infty}\frac{\alpha_l}{l+1}\frac{dP_l}{d\eta}\right)\hat{\mathbf{e}}_\theta. \tag{29}$$

The swimming velocity is evaluated using Lorentz reciprocal theorem [29] as

$$\mathbf{U_{s,0}} = \frac{-1}{4\pi}\iint_S \mathbf{u_{slip,0}}\, dA. \tag{30}$$

Substituting (29) in (30) we obtain the swimming velocity as

$$\mathbf{U}_{s,0} = \frac{-\mu}{(A+1)}\left(\frac{\alpha_1}{3} + A\right)\hat{\mathbf{e}}_z. \tag{31}$$

Here α_1 is the first mode of activity. Use of the Lorentz reciprocal theorem helps in determining the swimming velocity at O(Pe^0) without calculating the velocity field at O(Pe^0). However, to evaluate the swimming velocity at O(Pe), the velocity field must be evaluated at O(Pe^0), which arises as a source term in (18). The axisymmetric nature of the problem encourages us to seek the velocity field using a stream-function formulation. We define the stream function ψ_0 such that the radial and polar velocity components are given by

$$\mathbf{u}_r = -\frac{1}{r^2}\frac{\partial\psi_0}{\partial\eta}, \quad \mathbf{u}_\theta = -\frac{1}{r\sqrt{1-\eta^2}}\frac{\partial\psi_0}{\partial r}. \tag{32}$$

The stream function is obtained as

$$\psi_0 = U_{s,0}\left(r^2 - \frac{1}{r}\right)Q_1(\eta) + \frac{\mu}{2(A+1)}\sum_{n=2}^{\infty} n\alpha_n(r^{-n} - r^{2-n})Q_n(\eta). \tag{33}$$

We refer the readers to Appendix A for the detailed derivation of (33). The radial and polar components are evaluated using (32) as

$$\begin{aligned}
\mathbf{u}_{r,0} &= \mathbf{U}_{s,0}\left(\frac{1}{r^3} - 1\right)P_1(\eta) - \frac{\mu}{2(A+1)}\sum_{n=2}^{\infty} n\alpha_n(r^{-n-2} - r^{-n})P_n(\eta), \\
\mathbf{u}_{\theta,0} &= \frac{1}{\sqrt{1-\eta^2}}\left[-\mathbf{U}_{s,0}\left(2 + \frac{1}{r^3}\right)Q_1(\eta) + \frac{\mu}{2(A+1)}\sum_{n=2}^{\infty} n\alpha_n(nr^{-n-2} + (2-n)r^{-n})Q_n(\eta)\right].
\end{aligned} \tag{34}$$

Having determined the concentration and velocity field at $O(\mathrm{Pe}^0)$, we seek the solution of the system of Eqs. (18)–(23).

IV. SOLUTION OF CONCENTRATION FIELD AT O(Pe)

Forced convection types of problems such as the current problem are often singular in nature [21,22,24,30], i.e., the regular perturbation scheme introduced in (10) fails in the complete domain. We compare the leading order disturbance of concentration field of the advective and diffusive terms in the solute transport equation. From Eqs. (28) and (33) the leading order velocity and concentration fields scale as

$$\mathbf{u} \sim -\mathbf{U}_{s,0} + O(r^{-2}) \tag{35}$$

and

$$c_0 \sim A(r + U_s t) + O(r^{-1}). \tag{36}$$

From the solute transport equation, we note that the advective field decays as $\mathrm{Pe}\, r^{-2}$ while the diffusion decays as r^{-3}. The diffusive disturbance decays faster compared to the advective disturbance. Solute advection balances diffusion at a distance $r \sim \mathrm{Pe}^{-1}$. The limit $\mathrm{Pe} \to 0$ is therefore singular, i.e., there is a region far away from the particle where advection balances diffusion. An outer radial coordinate $\rho = \mathrm{Pe}\, r$ is introduced such that at distances $r \sim \mathrm{Pe}^{-1}$, $\rho \sim O(1)$ as $\mathrm{Pe} \to 0$. Writing (36) in terms of the outer variable suggests that the singularity in the concentration field appears at $O(\mathrm{Pe})$. The singular problem is solved via the classic method of matched asymptotic expansion. The complete domain is divided into an "inner region" close to the particle where diffusion dominates and an "outer region" far away [$r \sim O(\mathrm{Pe}^{-1})$] from the particle where advection balances diffusion. In the inner region, only the surface boundary condition is applied and the far field boundary condition is applied only in the outer region. The inner and the outer solutions are then matched via Van Dyke's principle [28].

A. Inner region

The solute concentration field close to the particle is governed by Eqs. (18) and (19). We have intentionally left the far field condition as it falls in the "outer region." To evaluate the source term in (18) the velocity from (34) is defined as

$$\mathbf{u}_0 = \sum_{n=1}^{\infty}\left(D_n(r)P_n(\eta)\hat{\mathbf{r}} + \frac{E_n(r)Q_n(\eta)}{\sqrt{1-\eta^2}}\hat{\theta}\right), \tag{37}$$

where

$$D_1(r) = -U_{s,0}\left(1-\frac{1}{r^3}\right) \quad \text{and} \quad D_n(r) = \frac{-\mu n\alpha_n(r^{-n-2}-r^{-n})}{2(A+1)} \quad \text{for } \forall n \neq 1,$$

and

$$E_1(r) = -U_{s,0}\left(2+\frac{1}{r^3}\right) \quad \text{and} \quad E_n(r) = \frac{\mu n\alpha_n(nr^{-n-2}+(2-n)r^{-n})}{2(A+1)} \quad \text{for } \forall n \neq 1.$$

Similarly, from (28) ∇c_0 is evaluated as

$$\nabla c_0 = \sum_{l=0}^{\infty}\left(F_l(r)P_l(\eta)\hat{\mathbf{r}} - \sqrt{1-\eta^2}G_l(\eta)\frac{dP_l}{d\eta}\hat{\theta}\right), \tag{38}$$

where

$$F_1(r) = A - \frac{A+\alpha_1}{r^3} \quad \text{and} \quad F_l(r) = \alpha_l r^{-(l+2)} \quad \text{for } \forall l \neq 1,$$

and

$$G_1(r) = A + \frac{A+\alpha_1}{2r^3} \quad \text{and} \quad G_l(r) = \frac{\alpha_l r^{-(l+2)}}{l+1} \quad \text{for } \forall l \neq 1.$$

From (37) and (38), the advective term is evaluated. This appears as a source term in (18). The source term is expressed as

$$\mathbf{u_0}\cdot\nabla c_0 = \sum_{k=0}^{\infty}\sum_{l=0}^{\infty}\sum_{n=1}^{\infty}[D_n(r)F_l(r)H_{nlk} + E_n(\eta)G_l(\eta)I_{nlk}]P_k(\eta). \tag{39}$$

Here, H_{nlk} and I_{nlk} determine the coupling between velocity and solute concentration field in the radial and the polar direction, respectively. H_{nlk} and I_{nlk} are defined as follows:

$$H_{nlk} = \frac{2k+1}{2}\int_{-1}^{1} P_n(\eta)P_l(\eta)P_k(\eta)d\eta, \tag{40}$$

$$\mathrm{I}_{nlk} = \frac{2k+1}{2n(n+1)}\int_{-1}^{1}\frac{dP_n}{d\eta}\frac{dP_l}{d\eta}P_k(\eta)(1-\eta^2)d\eta. \tag{41}$$

The unsteady term at $O(\mathrm{Pe})$ appears as another source term, which we represent as S_0:

$$S_0 = \frac{\partial c_0}{\partial t} = A\mathbf{U}_s. \tag{42}$$

Using the definition of $D_n(r)$, $F_l(r)$, $E_n(r)$, and $G_l(r)$, we represent the source term (39) ($\mathbf{u}_0\cdot\nabla c_0$) as a sum of four terms S_1, S_2, S_3, and S_4, defined below:

(1) S_1 containing the term with $n = 1, l = 1$ in (39),
(2) S_2 containing the terms with $n = 1$, ($l \geqslant 0$ except $l = 1$),
(3) S_3 containing the terms with $l = 1$ ($n \geqslant 2$), and
(4) S_4 containing the terms with ($n \geqslant 2$ and $l \geqslant 0$ except $l = 1$).

This takes into account all the possible terms in (39). We now evaluate the particular solution corresponding to each source term. The particular solution in the inner region is given by $c_p = c_{p,0} + c_{p,1} + c_{p,2} + c_{p,3} + c_{p,4}$. Here $c_{\mathrm{p.i}}$ represents the particular solution corresponding to the nonhomogeneity S_i .The particular solution corresponding to each term in the source S_i is of the form $r^s P_k(\eta)$. The specific solution corresponding to each source term is provided in Appendix B. The homogenous part of the solution to the Laplace equation is expressed in terms of growing and

decaying harmonics as

$$c_h = \sum_{k=0}^{\infty} (\hat{A}_k r^k + \hat{B}_k r^{-(k+1)}) P_k(\eta). \tag{43}$$

The complete inner solution is given by $c_1 = c_h + c_p$. Thus, we obtain

$$c_1 = \sum_{k=0}^{\infty} (\hat{A}_k r^k + \hat{B}_k r^{-(k+1)}) P_k(\eta) + c_p, \tag{44}$$

where c_p is the particular solution. The coefficients $\hat{A}_k, \hat{\mathrm{B}}_k$ must be evaluated using the boundary condition (19) and the matching condition with the outer solution.

B. Outer region

In the outer region we rescale the radial variable r to ρ as $\rho = \mathrm{Pe}\, r$. The outer region variables are denoted by a $\sim$. The velocity field given by (34) is rescaled by the outer coordinate. In terms of the rescaled variable ρ in the velocity field given by (34), is

$$\begin{aligned}
\tilde{\mathbf{u}}_r &= \mathbf{U}_{s,0}\left(\frac{\mathrm{Pe}^3}{\rho^3} - 1\right) P_1(\eta) - \frac{\mu}{2(A+1)} \sum_{n=2}^{\infty} n\alpha_n (\rho^{-n-2}\mathrm{Pe}^{n+2} - \rho^{-n}\mathrm{Pe}^n) P_n(\eta), \\
\tilde{\mathbf{u}}_\theta &= \frac{1}{\sqrt{1-\eta^2}} \Bigg[-\mathbf{U}_{s,0}\left(\frac{\mathrm{Pe}^3}{\rho^3} + 2\right) Q_1(\eta) + \frac{\mu}{2(A+1)} \\
&\qquad \times \sum_{n=2}^{\infty} n\alpha_n [n\rho^{-n-n}\mathrm{Pe}^{n+2} + (2-n)\rho^{-n}\mathrm{Pe}^n] Q_n(\eta) \Bigg].
\end{aligned} \tag{45}$$

In the limit $\mathrm{Pe} \to 0$, terms of the form Pe^m, $m \geqslant 1$ do not contribute in the velocity field. Thus the velocity field in the outer region, in the limit $\mathrm{Pe} \to 0$, is given by

$$\begin{aligned}
\tilde{\mathbf{u}}_r &= -\mathbf{U}_{s,0} P_1(\eta), \\
\tilde{\mathbf{u}}_\theta &= \frac{-2\mathbf{U}_{s,0} Q_1(\eta)}{\sqrt{1-\eta^2}}.
\end{aligned} \tag{46}$$

Substituting this velocity field in terms of outer variable in the advection diffusion equation and expressing the solute concentration in the outer region as $\tilde{c}(\rho, \eta)$ we obtain

$$\tilde{\nabla}^2 \tilde{c} = \frac{\partial \tilde{c}}{\partial t} - \mathbf{U}_s \eta \frac{\partial \tilde{c}}{\partial \rho} - \mathbf{U}_s \frac{(1-\eta^2)}{\rho} \frac{\partial \tilde{c}}{\partial \eta} \tag{47}$$

with the boundary condition

$$\tilde{c} \to \tilde{C}_\infty \quad \text{as} \quad \rho \to \infty. \tag{48}$$

Here the external field has also been rescaled as $\tilde{C}_\infty = A\rho\cos\theta + AU_s t$. Defining a steady disturbance concentration field, $\tilde{c}'(\rho, \eta) = \tilde{c}(\rho, \eta, t) - \tilde{C}_\infty(\rho, \eta, t)$, Eqs. (47) and (48) yield

$$\tilde{\nabla}^2 \tilde{c}' = -2\mathbf{U}_{s,0}\left(-A + \frac{\eta}{2}\frac{\partial \tilde{c}'}{\partial \rho} + \frac{(1-\eta^2)}{2\rho}\frac{\partial \tilde{c}'}{\partial \eta}\right). \tag{49}$$

We seek the outer solution in the limit $\mathrm{Pe} \to 0$ as an asymptotic expansion of the form

$$\tilde{c}'(\rho, \eta, \mathrm{Pe}) = \sum_{n=0}^{N} F_n(\mathrm{Pe}) \tilde{c}'_n(\rho, \eta), \tag{50}$$

where the gauge functions $F_n(\mathrm{Pe})$ are unknown and must satisfy

$$\frac{F_{n+1}}{F_n} \to 0 \quad \text{as} \quad \mathrm{Pe} \to 0.$$

Substituting (50) into (49) we find to leading order,

$$\tilde{\nabla}^2 \tilde{c}_0' = -2\mathbf{U}_{s,0}\left(-A + \frac{\eta}{2}\frac{\partial \tilde{c}_0'}{\partial \rho} + \frac{(1-\eta^2)}{2\rho}\frac{\partial \tilde{c}_0'}{\partial \eta}\right). \tag{51}$$

Following Subramanian [22] and Leal [31], the solution to (51) is given by

$$\tilde{c}_0' = A \exp\left(\frac{\mathbf{U}_{s,0}\rho\eta}{2}\right)\left(\frac{\pi}{\mathbf{U}_{s,0}\rho}\right)^{1/2}\left[\sum_{k=0}^{\infty} D_k K_{k+1/2}\left(\frac{\mathbf{U}_{s,0}\rho}{2}\right)P_k(\eta)\right]. \tag{52}$$

Here, $K_{k+\frac{1}{2}}(\frac{\mathbf{U}_{s,0}\rho}{2})$ is the modified Bessel function, as described in Abramowitz and Stegun [32]:

$$K_{k+1/2}\left(\frac{\mathbf{U}_{s,0}\rho}{2}\right) = \left(\frac{\pi}{\mathbf{U}_{s,0}\rho}\right)^{1/2} \exp\left(\frac{-\mathbf{U}_{s,0}\rho}{2}\right)\sum_{m=0}^{k}\frac{(k+m)!}{(k-m)!m!(\mathbf{U}_{s,0}\rho)^m}. \tag{53}$$

The coefficients D_k in (52) are determined using matching with the inner solution.

C. Matching

We first perform a leading order matching for the concentration field. In the limit $\mathrm{Pe} \to 0$, the outer solution at leading order, $F(\mathrm{Pe})\tilde{c}_0'$, must match with the inner solution at leading order c_0', that is,

$$F_0(\mathrm{Pe})\tilde{c}_0'|_{\rho\to 0} \Leftrightarrow c_0'|_{r\to\infty}. \tag{54}$$

In the limit $r \to \infty$, the inner region disturbance field expressed in the outer variable (ρ) is given by $c_0' \to \frac{\alpha_0 \mathrm{Pe}}{\rho}$. Using (54), it is clearly seen that $F_0(\mathrm{Pe}) = \mathrm{Pe}$. It follows then that

$$\tilde{c}_0'|_{\rho\to 0} \Leftrightarrow \frac{\alpha_0}{\rho}. \tag{55}$$

The inner solution when expressed in terms of the outer variable decays as $O(\rho^{-1})$. Comparing this to the outer solution given by (52) and (53) suggests that for all $k \geqslant 1$, $D_k = 0$. The only unknown coefficient (D_0) is found by matching with the inner solution. Thus we obtain

$$D_0 = \frac{\alpha_0 \mathbf{U}_{s,0}}{A\pi} \quad \text{and} \quad \mathrm{D}_k = 0 \ \forall k \geqslant 1. \tag{56}$$

By substituting Eq. (56) in Eqs. (52) and (53) we obtain the leading order outer solution as

$$\tilde{c}_0' = \frac{(\mathrm{Pe})\alpha_0 \exp\left(\frac{-\mathbf{U}_{s,0}\rho(1-\eta)}{2}\right)}{\rho} + O[F_1(\mathrm{Pe})]. \tag{57}$$

We will now perform $O(\mathrm{Pe})$ matching of the inner solution with the outer solution. The inner solution expanded up to $O(\mathrm{Pe})$ is given by $c_0' + \mathrm{Pe}(c_1)$. From (44), we see that all terms in the particular solution decay to zero in the limit $r \to \infty$, except the term corresponding to $l = 0$ in $c_{p,2}$. The homogenous solution in the inner region is composed of growing and decaying harmonics. The decaying harmonics do not contribute in the limit $r \to \infty$. Thus, $c_0' + \mathrm{Pe}(c_1)$ in the limit $r \to \infty$ is given by

$$(c_0' + \mathrm{Pe}c_1)|_{r\to\infty} = \frac{\alpha_0}{r} + \mathrm{Pe}\left(\frac{\alpha_0 \mathbf{U}_{s,0}}{2}P_1(\eta) + \sum_{k=0}^{\infty}\hat{A}_k r^k P_k(\eta)\right). \tag{58}$$

The above equation must match with the outer solution in the limit $\rho \to 0$. The outer solution from Eqs. (57), (50), and expanded in the limit $\rho \to 0$, containing terms of $O(\mathrm{Pe})$ is given by

$$\tilde{c}'|_{\rho\to 0} = \frac{\mathrm{Pe}\alpha_0}{\rho}\left(1 - \frac{\mathbf{U}_{s,0}\rho(1-\eta)}{2}\right) + O[F_1(\mathrm{Pe})]. \tag{59}$$

Comparing (59) with (58) we obtain

$$\hat{A}_0 = -\frac{\alpha_0 \mathbf{U}_{s,0}}{2} \quad \text{and} \quad \hat{A}_k = 0 \ \forall k \geqslant 1. \tag{60}$$

Thus the solute concentration field in the inner region at $O(\mathrm{Pe})$ is given by

$$c_1 = \frac{-\alpha_0 \mathbf{U}_{s,0}}{2} + \sum_{k=0}^{\infty} \hat{B}_k r^{-(k+1)} P_k(\eta) + c_p. \tag{61}$$

Note that the first term changes the solute concentration throughout the domain. As the slip velocity is proportional to surface gradient, it does not have any effect on the particle dynamics. Based on Van Dyke's matching [28], the composite solution for the concentration field is given by $c_{\mathrm{comp}} = c_1 + \tilde{c}' - (\tilde{c}')|_{\rho\to 0}$. However, as the slip velocity at the particle surface lies in the inner region, we use only the inner solution to find the slip velocity. We now use the surface boundary conditions to determine $\hat{B}_k$. We refer the readers to Appendix C for the detailed derivation and expression for each $\hat{B}_k$.

V. RESULTS AND DISCUSSION

The slip velocity at $O(\mathrm{Pe})$ is evaluated using $\mathbf{u}_{s,1} = \frac{\mu(\mathbf{I}-\mathbf{nn})\cdot\nabla c_1}{A+1}$. Substituting this expression in the Lorentz reciprocal theorem, we obtain the swimming velocity as

$$\mathbf{U}_{s,1} = \frac{1}{2}\int_1^{-1} \mu(1-\eta^2)\frac{dc_1}{d\eta}\bigg|_{r=1} d\eta. \tag{62}$$

In the above Eq. (62), $(1-\eta^2)$ can be written as a sum of two Legendre polynomials [$P_0(\eta)$ and $P_2(\eta)$]. Using the orthogonality property of Legendre polynomials, we conclude that only two modes of the term $\frac{dc_1}{d\eta}$ contribute to the correction in swimming velocity. We now present results of three specific cases: (i) a Janus particle with surface activity $\alpha(\eta) = \frac{-1-\eta}{2}$, (ii) half-coated Janus particle, and (iii) non-half-coated Janus particle as shown in Fig. 2.

A. Janus particle with surface activity of the form $\alpha(\eta) = \frac{-1-\eta}{2}$

This form of surface activity leads to a closed form solution with far less numbers of terms compared to other two cases. Here, a Janus-like particle has a surface activity given by

$$\alpha = \frac{-1-\eta}{2}. \tag{63}$$

The negative value of surface activity signifies that solute particles are consumed at the particle surface. The magnitude of surface activity is maximum at the front pole ($\theta = 0$) and it continuously decreases to zero at the rear pole ($\theta = \pi$). This form of surface activity significantly simplifies the algebra and helps obtain a closed form expression for swimming velocity and $O(\mathrm{Pe})$ concentration field. The leading order concentration field is given by

$$c_0 = Ar\eta + \frac{A\eta}{2r^2} - \frac{1}{2r} - \frac{\eta}{4r} + AU_s t. \tag{64}$$

Figure 3(a) shows the concentration field around a particle with activity distribution given by (63). Figure 3(a) shows that this activity distribution gives rise to a qualitatively similar concentration field as a Janus particle [19,27,30]. Solute particles are adsorbed towards the front pole of the

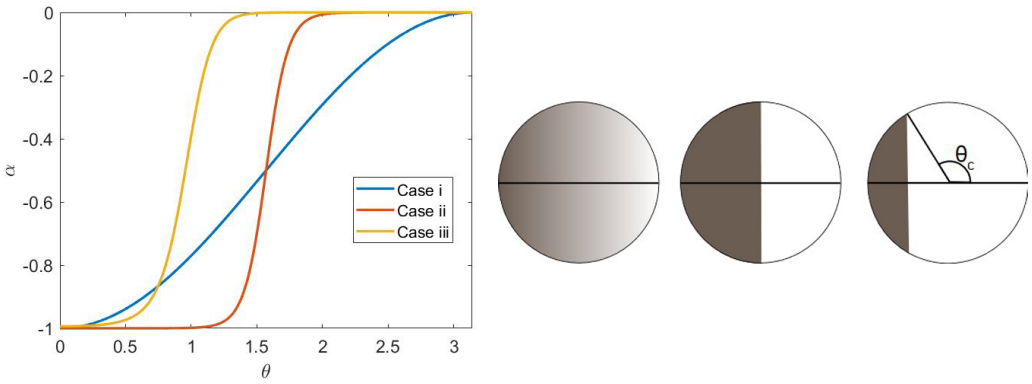

(a) (b)

FIG. 2. Surface activity as a function of polar angle θ for the cases (i) $\alpha(\theta) = \frac{-1-\cos\theta}{2}$, (ii) half-faced surface activity, and (iii) non-half-sigmoidal surface activity. (b) depicts surface activity distribution on the particle surface. Surface activity corresponding to white and gray color is -1 and 0, respectively. θ_c corresponds to the transition polar angle, and we take $\theta_c = \cos^{-1}(\frac{-1}{\sqrt{3}})$.

particle, which results in a drop in concentration there. For a positive (negative) value of mobility coefficient, this particle will move towards the right (left). Figure 3(b) shows the particle placed in an external concentration gradient with $A = 0.25$. The external concentration gradient is stronger than the local concentration gradient. This results in a reversal in the direction of global concentration gradient. Consequently, the direction of motion changes from positive (right) to negative (left) z direction. Using the Lorentz reciprocal theorem, the leading order swimming velocity is evaluated as

$$U_{s,0} = \mu\left(\frac{1}{6(A+1)} - \frac{A}{A+1}\right). \tag{65}$$

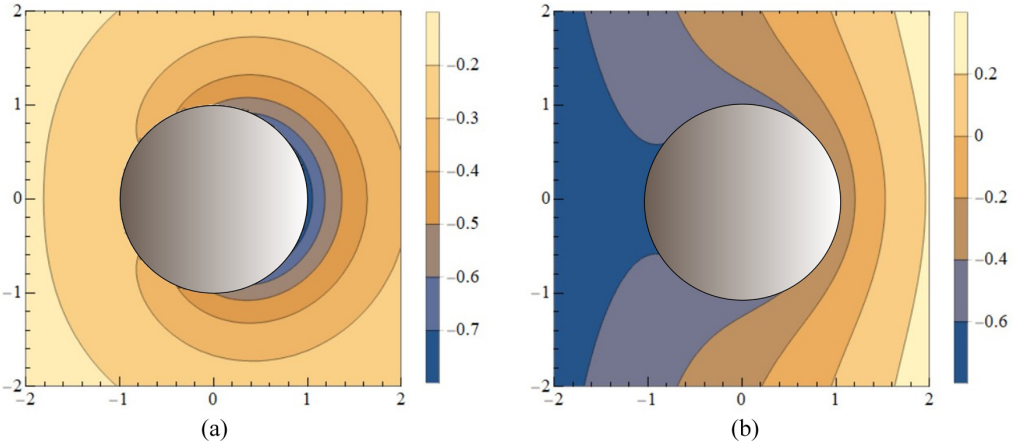

(a) (b)

FIG. 3. Concentration field around the particle for the case Pe $= 0$ for (a) $A = 0$ and (b) $A = 0.25$. Surface activity corresponding to white and gray color is -1 and 0, respectively. The solute molecules are getting consumed at the front end in panel (a) The concentration field is axisymmetric in nature. The external gradient dominates the local gradient for the second case (b) and reverses the net concentration gradient.

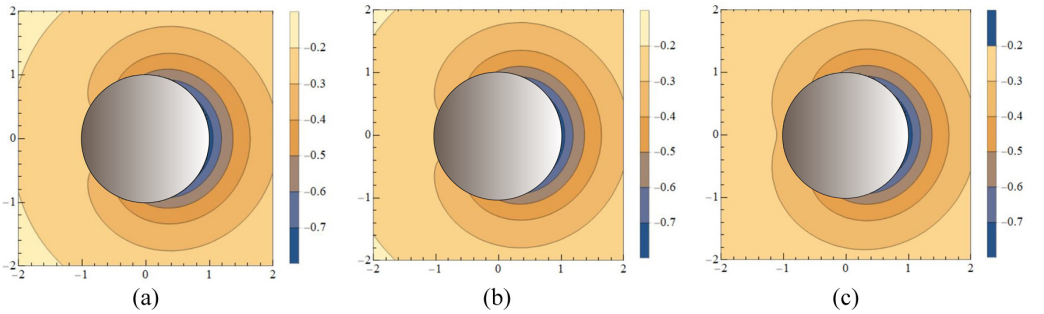

FIG. 4. Solute concentration contours for (a) Pe = 0.25, (b) Pe = 0.5, and (c) Pe = 0.75 for $\mu = 1$ and $A = 0$. The fluid flow around the particle carries the low concentrated fluid from the front end ($\theta = 0$) to the rear end. This results in reduction in the difference of concentration at front and rear pole.

Following the methods discussed in preceding sections, $O(\mathrm{Pe})$ correction to the concentration field is evaluated as

$$c_1 = -\frac{\alpha_0 U_{s,0}}{2} + \frac{U_{s,0}(2A-1)}{12}\left(\frac{1}{r} - \frac{1}{4r^4}\right) + \frac{U_{s,0}}{4}\left(\frac{3}{4r^2} - 1 - \frac{1}{2r^3}\right)P_1(\eta) + \frac{U_{s,0}}{12}\left(\frac{8A-3}{3r^3} - \frac{4A-1}{r} - \frac{2A-1}{2r^4}\right)P_2(\eta). \tag{66}$$

The solution is shown as a contour plot in Fig. 4 for various Pe numbers. For a positive value of mobility coefficient, the particle has a positive swimming velocity. The fluid takes the solute molecules from the front towards the rear end of the particle. This results in a lower concentration of solute molecules compared to the case with no advection (Pe = 0). Consequently, the surface concentration gradient is reduced, which leads to a reduction in swimming velocity. This observation is qualitatively consistent with the result of Michelin and Lauga [19].

We quantify the reduction in swimming velocity using the Lorentz reciprocal theorem (62) with (66). Substituting (66) in (62) we obtain the correction in swimming velocity as

$$U_{s,1} = -\frac{\mu U_{s,0}}{8(A+1)}, \tag{67}$$

where $U_{s,0}$ is given by (65). The correction is proportional and opposite to the swimming velocity. The net swimming velocity up to $O(\mathrm{Pe})$ is given by

$$U_s = U_{s,0}\left(1 - \frac{\mu \mathrm{Pe}}{8(A+1)}\right). \tag{68}$$

It is important to note that the correction at $O(\mathrm{Pe})$ is proportional to μ^2(as $U_{s,0}$ is also proportional to μ). Thus the correction to the swimming velocity is independent of the sign of the mobility coefficient. Additionally, $O(\mathrm{Pe})$ correction always reduces the magnitude of the swimming velocity. This is shown in Fig. 5(a), where the magnitude of the swimming velocity reduces for both positive and negative mobility. The swimming velocity at the leading order is a function of activity number A. Consequently, the correction to the swimming velocity is an implicit function of A. As A is increased, the correction reduces, in the limit $A \to \infty$, and the correction tends to zero.

B. Half-coated Janus particle

We now look at the case of a half-coated Janus particle. The surface activity of a half-coated Janus particle changes sharply at $\theta = 0$. Expressing a steplike function in Legendre polynomial basis leads to a very slowly convergent series for the $O(\mathrm{Pe})$ correction. This increases the computational

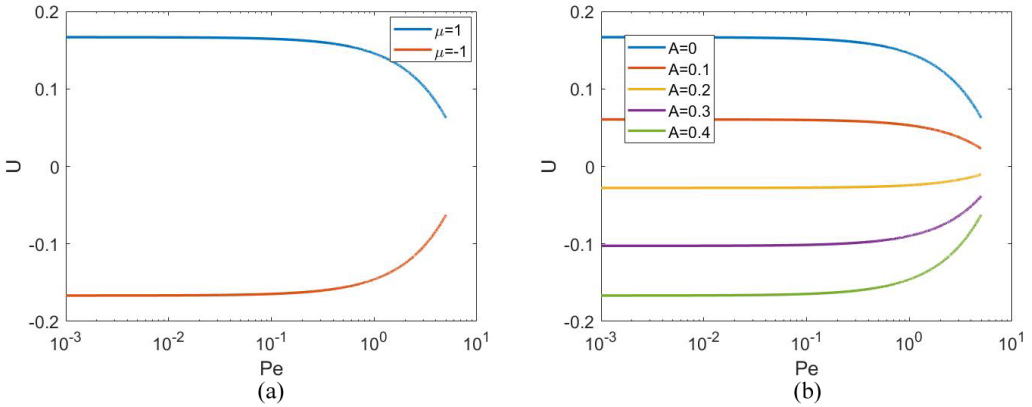

FIG. 5. The swimming velocity variation with Péclet number. (a) shows the swimming velocity for positive and negative mobility for $A = 0$. In both cases, $O(\mathrm{Pe})$ effect reduces the magnitude of the swimming velocity. (b) shows the swimming velocity for different activity numbers and $\mu = 1$. The correction is proportional and opposite to the leading order swimming velocity.

power needed to evaluate the corrected concentration field, slip velocity, and swimming velocity. To overcome this, we approximate the surface coverage with a smoothly varying sigmoidal function:

$$\alpha = f(\eta) = \frac{-\exp(m\eta)}{1+\exp(m\eta)}. \tag{69}$$

Here, m (transitional parameter) determines the sharpness of the activity function, and $\eta = \cos\theta$. This introduces an additional length scale in the system, which scales as $l_c = \frac{4a^*}{m}$. For $m = 12$, the characteristic length scale for a particle of size $10\,\mu$m is $\sim 3\,\mu$m. As shown in Fig. 6, a higher value of m leads to a better approximation but increases computational power, while a lower value to m leads to a poor approximation. To balance both the accuracy and the computational power, in all analysis we choose $m = 12$. However, the methodology discussed in preceding sections is

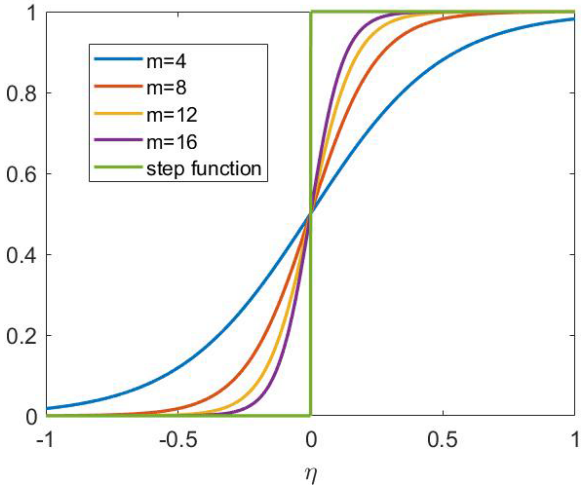

FIG. 6. Approximation of step function surface activity as a function of $\eta(\cos\theta)$. Increase in transitional parameter increases the sharpness and leads to better approximation of a step function. A negative activity signifies solute adsorption on the surface.

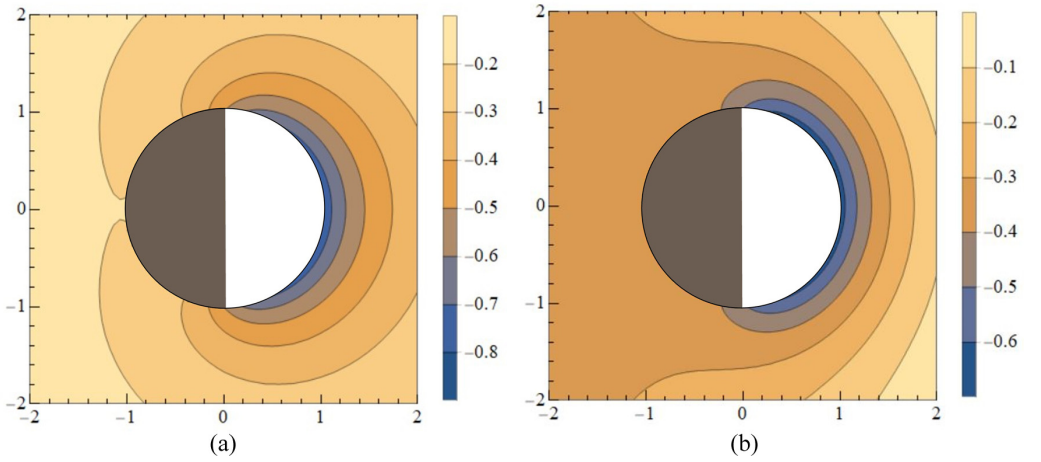

FIG. 7. Concentration contours around a particle with sigmoidal surface activity, for $m = 12$. Surface activity corresponding to white and gray color is -1 and 0, respectively. (a) shows the contour for $A = 0$, while in (b) $A = 0.1$. The direction of concentration gradient is towards the right, and it reduces the net concentration gradient, and consequently the swimming velocity.

applicable for any value of m. The leading order concentration field around a particle having surface activity expressed as (69) with $m = 12$ is given by (28) with $\alpha_l = \frac{(2l+1)}{2}\int_{-1}^{1} f(\eta)P_l(\eta)d\eta$ as the lth activity mode.

We approximate (28) by truncating the infinite series to a finite number of modes. The surface concentration as a function of η and the concentration field as a function of distance (r) is shown in Fig. 8 for $A = 0$. As seen in Figs. 8(a) and 8(b), the surface concentration and the concentration field as a function of r for 20 modes overlaps completely for ten modes. Thus we conclude that the solution has converged for ten modes, and we use ten modes in (28) for our analysis.

The solute concentration field is shown in Fig. 7(a) for the case $A = 0$ and Fig. 7(b) with external concentration gradient ($A = 0.1$). As seen in Fig. 7(b), the external concentration gradient opposes the self-generated concentration gradient, resulting in a decrease in magnitude of surface gradient. This leads to reduction in slip velocity and consequently reduction of the swimming velocity at the leading order. The first order correction to concentration field is evaluated using (61). The net concentration field up to $O(\mathrm{Pe})$ is shown in Figs. 9(a)–9(c) for Péclet numbers 0, 0.25, and 0.5, respectively.

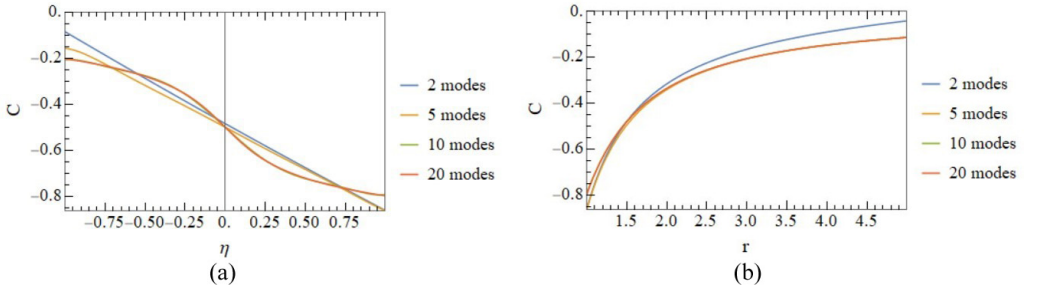

FIG. 8. Surface concentration is shown for different numbers of modes for $A = 0$, $\mathrm{Pe} = 0.5$, where (b) shows the decaying concentration field as a function of r. It is clearly visible that the surface concentration has converged at ten modes.

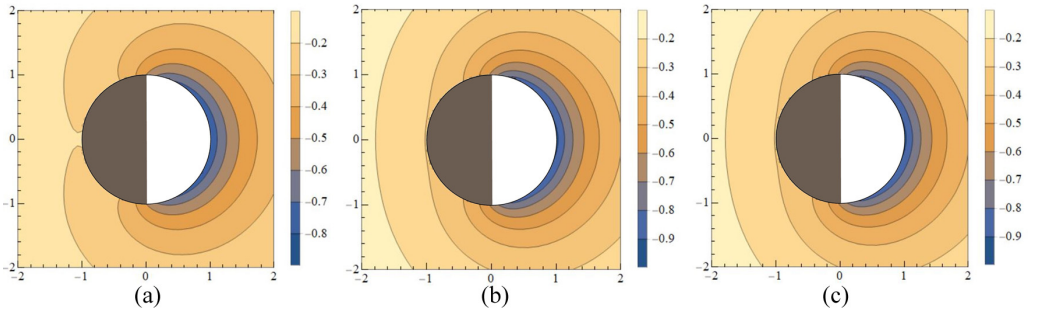

FIG. 9. Solute concentration contour for (a) Pe = 0, (b) Pe = 0.25, and (c) Pe = 0.5 with $\mu = 1$. The solute advection transports the fluid with low concentration to the inert side of the particle. This reduces the difference between the concentration difference between the active and inert half.

Figures 9(a)–9(c) show the concentration contours for Pe = 0, 0.25, and 0.5, respectively. Here again, the solute advection transports solute from the front pole ($\theta = 0$) in Fig. 9(a) towards the rear pole ($\theta = \pi$). We now look at the swimming velocity obtained from our analysis. For a positive mobility ($\mu = 1$), the leading order swimming velocity obtained using the Lorentz reciprocal theorem is given by

$$U_{s,0} = \frac{0.2442}{A+1} - \frac{A}{A+1}, \tag{70}$$

and $O(\mathrm{Pe})$ correction is given by

$$U_{s,1} = -\frac{U_{s,0}}{8(A+1)}. \tag{71}$$

The net swimming velocity is obtained as

$$U_s = U_{s,0}\left(1 - \frac{\mathrm{Pe}}{8(A+1)}\right). \tag{72}$$

Note that the relation for the corrected velocity is the same as obtained for the previous simple case. However, the expression for $U_{s,0}$ is different for a Janus particle. Figure 10(a) shows the swimming velocity for different values of the transition parameter (m). As the value of transition parameter m increases, the swimming velocity expression gets closer to a Janus particle with sharp variation in activity obtained numerically by Michelin and Lauga [19]. As shown in Fig. 10(a), the velocity expression given in (72) matches well with numerical results of Michelin and Lauga [19] up to $\mathrm{Pe} \sim 1$, in spite of the assumption of $\mathrm{Pe} \ll 1$. Figure 10(b) shows the relation of swimming velocity with the activity number.

Here again, the correction is independent of nature of molecular interactions characterized by μ. Additionally, the correction reduces the swimming velocity for both kinds of interactions. The limit $A \to \infty$ corresponds to a neutral particle placed in the external gradient. In this limit, the correction tends to zero as observed by previous studies [21,24].

C. Non-half-coated Janus particle

We now consider a non-half Janus particle. The surface activity for a non-half particle is expressed similar to (69). For a non-half Janus particle with activity transitioning at θ_c, we shift (69) by $\eta_c = \cos\theta_c$. The surface activity is given by

$$\alpha = g(\eta) = \frac{-\exp\left[m(\eta - \eta_c)\right]}{1 + \exp\left[m(\eta - \eta_c)\right]}. \tag{73}$$

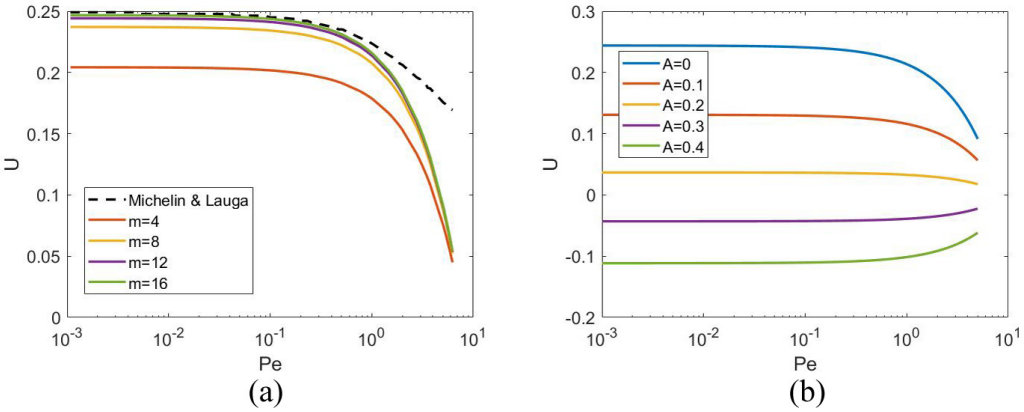

FIG. 10. Variation of swimming velocity with Péclet number for (a) different transitional parameter and (b) for different A. (a) also serves as verification of our results; the swimming velocity approaches the results of Michelin and Lauga [19] as m is increased. Swimming velocity as a function of activity number is shown in (b). The advective effects reduce the magnitude of swimming velocity for all values of activity number.

The negative sign in (73) refers to consumption of the solute molecules on the surface. We consider the transition occurs at $\eta_c = \frac{-1}{\sqrt{3}}$. The leading concentration field is given by (28) with $\alpha_l = \frac{(2l+1)}{2}\int_{-1}^{1} g(\eta)P_l(\eta)d\eta$. We truncate the leading order solution (28) again at $l = 9$ (ten modes). The leading concentration field for this case with $m = 12$ is shown in Fig. 11. As shown in the figure, the effect of the external concentration gradient is to oppose the self-generated concentration gradient. As activity number increases, the relative strength of external concentration gradient increases. At $A = 0.5$, the external concentration gradient dominates the local concentration gradient. Using the Lorentz reciprocal theorem, we evaluate the leading order swimming velocity.

For a particle with positive mobility, the swimming velocity expression is

$$U_{s,0} = \frac{0.1612}{A+1} - \frac{A}{A+1}, \tag{74}$$

whereas for a non-half Janus particle with $\eta_c = \frac{-1}{\sqrt{3}}$ and in the absence of external concentration gradient, the swimming velocity is $\frac{1}{6}$. As the value of the transition parameter increases, the

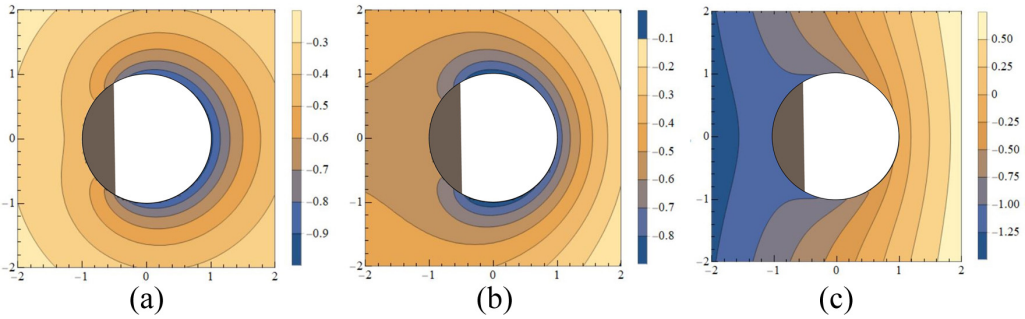

FIG. 11. Concentration field for a non-half Janus particle for (a) $A = 0$, (b) $A = 0.1$, and (c) $A = 0.5$ with $m = 12$. Surface activity corresponding to white and gray color is -1 and 0, respectively. The effect of concentration gradient is to oppose the self-generated concentration gradient. At $A = 0.5$, the external concentration gradient dominates the local concentration gradient.

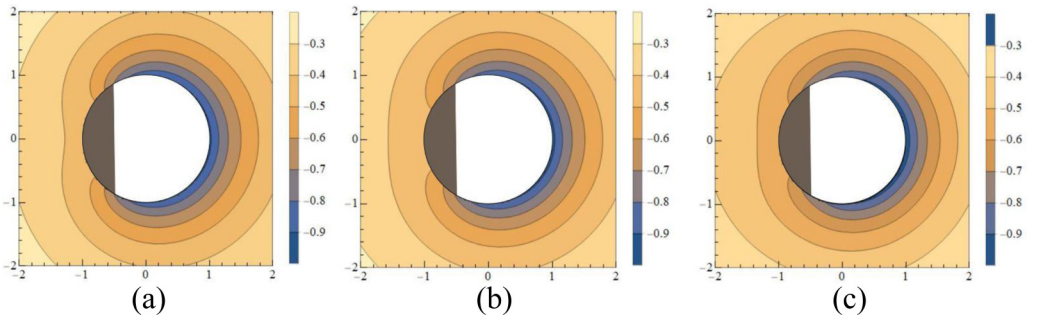

FIG. 12. Effect of solute advection on the concentration field for a particle with positive mobility for (a) Pe = 0, (b) Pe = 0.25, and (c) Pe = 0.75. Solute advection brings the solute deficient region towards the inert pole, reducing the magnitude of difference of concentration between the front and rear pole. As Pe increases, more solute is brought from the active face towards the inert face.

swimming velocity approaches the swimming velocity of a non-half particle with a sharp transition. The effect of solute advection characterized by Péclet number is shown in Fig. 12. The difference in surface concentration at the front and rear pole reduces from 0.5 for Pe = 0 to 0.4 for Pe = 0.75. This shows a reduction in surface concentration gradient, which results in a slower slip velocity. Using the Lorentz reciprocal theorem, we get an expression for swimming velocity at $O(\mathrm{Pe})$ given by

$$U_{s,1} = \frac{-0.032}{(A+1)^2} + \frac{0.144}{(A+1)^2}. \tag{75}$$

This can be reasonably approximated as

$$U_{s,1} = -\left(\frac{U_{\mathrm{self}}}{5(A+1)} + \frac{U_{\mathrm{ext}}}{7(A+1)}\right), \tag{76}$$

where $U_{\mathrm{self}} = \frac{0.1612}{(A+1)}$ and $U_{\mathrm{ext}} = \frac{-A}{A+1}$. Comparing this result with (71), we observe that for a half-coated particle, the correction depends equally on both the components, whereas for a non-half Janus

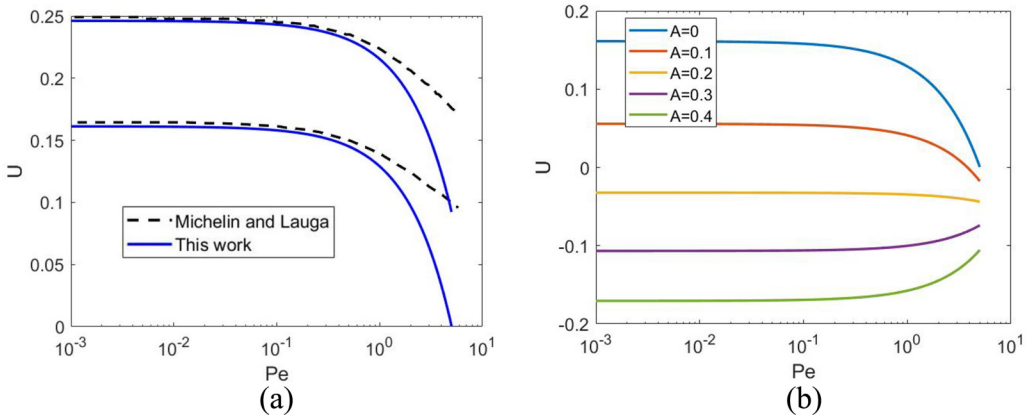

FIG. 13. Swimming velocity as a function of Péclet number. (a) compares the result obtained by numerical investigation of Michelin and Lauga [19] (shown by black dashed lines) for $A = 0$ with the current framework for half and non-half particle. (b) shows the swimming velocity for different activity numbers.

particle, two components contribute unequally. Combining (76) and (74), the complete swimming velocity up to $O(\mathrm{Pe})$ is given by

$$U_s = \frac{0.1612}{A+1} - \frac{A}{A+1} + \mathrm{Pe}\left(\frac{-0.032}{(A+1)^2} + \frac{0.144A}{(A+1)^2}\right). \tag{77}$$

The direction of motion at leading order reverses at $A = 0.162$, while the correction reverses the direction at $A = 0.223$. Therefore, when $0.1612 \leqslant A \leqslant 0.223$, the solute advection gives rise to increase in swimming velocity. The effect of solute advection is to reduce the swimming velocity when $A \geqslant 0.223$ and $A \leqslant 0.1612$. This is seen in Fig. 13(b), where solute advection reduces the swimming velocity for $A = 0,\ 0.1,\ 0.3$, and 0.4, whereas when $A = 0.2$ it lies in the range $0.1612 \leqslant A \leqslant 0.223$; solute advection increases the swimming velocity. In this range of A, the solute advection increases the surface concentration gradient. This results in a higher slip and swimming velocity. For the swimming velocity in terms of the contribution of both the effects, the expression is given by

$$U_s = U_{\mathrm{self}} + U_{\mathrm{ext}} - \mathrm{Pe}\left(\frac{U_{\mathrm{self}}}{5(A+1)} + \frac{U_{\mathrm{ext}}}{7(A+1)}\right). \tag{78}$$

Figure 13(a) shows our asymptotic analysis compares favorably with the numerical study of Michelin and Lauga [19] for the case $A = 0$ up to $\mathrm{Pe} \sim 0.5$.

VI. CONCLUSIONS

In this study we have investigated the effect of solute advection on the swimming velocity of an active particle under the influence of an external concentration gradient. We quantify the role of solute advection once the particle has reoriented along the external concentration gradient. We assume the solute concentration is high, resulting in a constant rate of reaction on the active face. The Péclet number which characterizes these systems is typically small $[O(10^{-2})]$ [5,6]. We provide a theoretical framework quantifying $O(\mathrm{Pe})$ corrections to the swimming velocity of an active particle with axisymmetric distribution of surface activity. We use a singular perturbation scheme along with the method of matched asymptotics to obtain the solute concentration field in a closed form. We employ Lorentz reciprocal theorem to evaluate $O(\mathrm{Pe})$ corrections to the swimming velocity.

Our analysis reveals that the correction in swimming velocity is seen at $O(\mathrm{Pe})$, in contrast to $O(\mathrm{Pe}^2)$ corrections seen for an inert particle [21]. The correction in swimming velocity is shown to reduce the swimming velocity of the particle. However, $O(\mathrm{Pe})$ corrections are modest. The reduction in swimming velocity for a half-faced active particle is proportional to the swimming velocity at the leading order. Specifically, the reduction is of the form $U_{s,1} = -\frac{U_{s,0}}{8(A+1)}$, where $U_{s,0}$ is the swimming velocity at the leading order. We also show that a simple model with surface activity of the form $\alpha(\theta) = \frac{-1-\cos\theta}{2}$ is sufficient to obtain an identical relation. As the magnitude of external gradient increases, the relative magnitude of the correction at $O(\mathrm{Pe})$ reduces. In the limit $A \to \infty$, which physically translates to the case of an inert particle, the correction tends to zero. This is in agreement with previous work [21,24], whereas for a non-half particle, $O(\mathrm{Pe})$ correction to the swimming velocity is proportional to a linear combination of U_{self} and U_{ext}. The contribution due to surface activity is larger than that due to external gradient in the corrected swimming velocity.

The analytical result obtained for both half and non-half surface activity coverage matches well with the numerical result reported by Michelin and Lauga [19]. Solute advection transports the solute molecules near the active surface towards the inert surface, thus reducing the concentration gradient. This results in a reduction in its swimming velocity.

This study derives a closed form solution to the concentration field and swimming velocity to account for weak advective effects up to $O(\mathrm{Pe})$. Recent studies [33–35] have shown the complex collective behavior of such particles, and this study will help analyze this. This study also helps in developing control strategies for applications such as drug delivery, cargo transport, etc.

APPENDIX A: EVALUATION OF STREAM FUNCTION

The stream function satisfies the biharmonic equation

$$\nabla^4 \psi_0 = 0. \tag{A1}$$

The general solution of this equation is given by

$$\psi_0 = \sum_{n=1}^{\infty} (A_n r^{n+3} + B_n r^{n+1} + C_n r^{2-n} + D_n r^{-n}) Q_n(\eta), \tag{A2}$$

where $Q_n(\eta)$, the Gegenbauer polynomial of order n and degree $-1/2$, is defined as $Q_n(\eta) = \int_{-1}^{\eta} P_n(x)dx$. The constants appearing in (A2) are determined using the boundary conditions (16) and (17). Using the far field condition (16), we obtain

$$A_n = 0 \ \forall n \quad \text{and} \quad B_n = 0 \ \forall n \neq 1, B_1 = U_{s,0}. \tag{A3}$$

Using the boundary condition (17) and the solution to c_0 from (28), we obtain

$$D_n = -C_n \quad \text{and} \quad D_n = \frac{\mu \alpha_n n}{2(A+1)} \quad \text{for} \quad \text{n} \geqslant 2. \tag{A4}$$

The swimming of Janus particle is force free and torque free. The Stokeslet contribution to the velocity field does not contribute, i.e., $C_1 = 0$ and $D_1 = -U_{s,0}$.

APPENDIX B: PARTICULAR SOLUTION CORRESPONDING TO THE SOURCE TERM

The particular solution corresponding to the nonhomogeneity S_i is given by $c_{p,i}$. The solutions corresponding to source term S_i is assumed to be of the form $\beta r^s P_k(\eta)$. After the application of Laplace operator, the assumed solution is compared to the source S_i to evaluate β. The solution corresponding to each source term is given as follows:

For the nonhomogeneity $S_0 + S_1$, the particular solution is

$$c_{p,0} + c_{p,1} = \left[-\frac{(A+\alpha_1)}{24} \cdot \frac{\mathbf{U}_s}{r^4} - \mathbf{U}_s \left(\frac{A+\alpha_1}{12r^4} + \frac{2A+\alpha_1}{6r} \right) P_2(\eta) \right]. \tag{B1}$$

For the nonhomogeneity S_2, the particular solution is

$$c_{p,2} = \mathbf{U}_s \alpha_l \left(\frac{\left(H_{1lk} - \frac{I_{1lk}}{l+1}\right) r^{-(l+3)}}{(l+3)(l+2) - k(k+1)} - \frac{\left(H_{1lk} + \frac{2}{l+1} I_{1lk}\right) r^{-l}}{l(l-1) - k(k+1)} \right) P_k(\eta). \tag{B2}$$

For the nonhomogeneity S_3, the particular solution is

$$\begin{aligned} c_{p,3} = \frac{\mu n \alpha_n}{2(A+1)} \Bigg(& \frac{A(-H_{n1k} + nI_{n1k}) r^{-n}}{n(n-1) - k(k+1)} + \frac{A[H_{n1k} + (2-n)I_{n1k}] r^{2-n}}{(n-2)(n-3) - k(k+1)} \\ & + \frac{(A+\alpha_1)\left(H_{n1k} + \frac{n}{2} I_{n1k}\right) r^{-n-3}}{(n+2)(n+3) - k(k+1)} + \frac{(A+\alpha_1)\left(-H_{n1k} + \frac{(2-n)}{2} I_{n1k}\right) r^{-n-1}}{n(n+1) - k(k+1)} \Bigg) P_k(\eta). \end{aligned} \tag{B3}$$

For the nonhomogeneity S_4, the particular solution is

$$c_{p,4} = \frac{\mu n \alpha_n \alpha_l}{2(A+1)} \left(\frac{\left(H_{nlk} + \frac{n}{l+1} I_{nlk}\right) r^{-(n+l+2)}}{(n+l+1)(n+l+2) - k(k+1)} - \frac{\left(H_{nlk} - \frac{(2-n)}{l+2} I_{nlk}\right) r^{-(n+l)}}{(n+l)(n+l+1) - k(k+1)} \right) P_k(\eta). \tag{B4}$$

APPENDIX C: EXPRESSION FOR EACH $\hat{B}_k$

Here we evaluate the coefficients $\hat{B}_k$ of the decaying harmonics in the homogenous solution. Substituting (61) in the no-flux boundary condition given by (19) at the surface of the particle, we

find the following:

$$B_0 = \left[\frac{(A+\alpha_1)U_{s,0}}{6} + \frac{\mu n\alpha_n\alpha_m}{2(A+1)}\left(\frac{H_{nl0} - \frac{nI_{nl0}}{l+1}}{n+l+1} - \frac{H_{nl0} + \frac{(2-n)I_{nl0}}{l+2}}{n+l-1}\right)\right]. \tag{C1}$$

$$\begin{aligned} B_2 = \left(\frac{1}{3}\right)\Bigg(&\frac{4A+3\alpha_1}{6}U_{s,0} - U_{s,0}\alpha_l\left(\frac{\left(H_{1l2} - \frac{I_{1l2}}{l+1}\right)(l+3)}{(l+2)(l+3)-6} - \frac{\left(H_{1l2} + \frac{2}{l+1}I_{1l2}\right)l}{l(l-1)-6}\right) \\ &+ \frac{\mu\alpha_n}{2(A+1)}\left(\frac{A(2-n)[H_{nl2} + (2-n)I_{nl2}]}{(n-2)(n-3)-6} - \frac{An(nI_{nl2} - H_{nl2})}{n(n-1)-6}\right) \\ &- \frac{\mu\alpha_n}{2(A+1)}\left(\frac{(A+\alpha_1)(n+1)\left[\left(\frac{2-n}{2}\right)I_{nl2} - H_{nl2}\right]}{n(n+1)-6} + \frac{(A+\alpha_1)(n+3)\left(H_{nl2} + \frac{n}{2}I_{nl2}\right)}{(n+2)(n+3)-6}\right) \\ &- \frac{\mu\alpha_n\alpha_l n}{2(A+1)}\left(\frac{\left[\left(\frac{n}{l+1}\right)I_{nl2} - H_{nl2}\right](n+l+2)}{(n+l+1)(n+l+2)-6} + \frac{\left[\left(\frac{2-n}{l+1}\right)I_{nl2} + H_{nl2}\right](n+l)}{(n+l)(n+l-1)-6}\right)\Bigg). \end{aligned} \tag{C2}$$

For $k \neq 0, 2$,

$$\begin{aligned} \hat{B}_k = \frac{1}{k+1}\Bigg(&-U_{s,0}\alpha_l\left(\frac{\left(H_{1lk} - \frac{I_{1lk}}{l+1}\right)(l+3)}{(l+2)(l+3)-k(k+1)} - \frac{\left(H_{1lk} + \frac{2I_{1lk}}{l+1}\right)l}{l(l-1)-k(k+1)}\right) \\ &+ \frac{-\mu n\alpha_n\alpha_l}{2(A+1)}\left(\frac{\left(\frac{n}{l+1}I_{nlk} - H_{nlk}\right)(n+l+2)}{(n+l+1)(n+l+2)-k(k+1)} + \frac{\left(\frac{2-n}{l+1}I_{nlk} - H_{nlk}\right)(n+l)}{(n+l)(n+l-1)-k(k+1)}\right) \\ &+ \frac{\mu n\alpha_n}{2(A+1)}\left(\frac{A(2-n)[H_{n1k} + (2-n)I_{n1k}]}{(n-2)(n-3)-k(k+1)} - \frac{An(-H_{n1k} + nI_{n1k})}{n(n-1)-k(k+1)}\right) \\ &- \frac{\mu n\alpha_n}{2(A+1)}\left(\frac{(A+\alpha_1)(n+1)\left(-H_{n1k} + \frac{(2-n)}{2}I_{n1k}\right)}{n(n+1)-k(k+1)} + \frac{(A+\alpha_1)(n+3)\left(H_{n1k} + \frac{n}{2}I_{n1k}\right)}{(n+2)(n+3)-k(k+1)}\right)\Bigg). \end{aligned} \tag{C3}$$

The above expressions (C1)–(C3) are summed over both n and l for each $\hat{B}_k$. The correction of concentration field at $O(\mathrm{Pe})$ is thus given by (61) with the constant factors ($\hat{B}_k$) evaluated using (C1)–(C3) and c_p obtained from (B1) to (B4).

[1] E. M. Purcell, Life at low Reynolds number, Am. J. Phys. **45**, 3 (1977).

[2] C. Brennen and H. Winet, Fluid mechanics of propulsion by cilia and flagella, Annu. Rev. Fluid Mech. **9** 339 (1977).

[3] E. Lauga and T. R. Powers, The hydrodynamics of swimming microorganisms, Rep. Prog. Phys. **72**, 096601 (2009).

[4] W. F. Paxton, S. Sundararajan, T. E. Mallouk, and A. Sen, Chemical locomotion, Angew. Chemie-Int. Ed. **45**, 5420 (2006).

[5] J. R. Howse, R. A. L. Jones, A. J. Ryan, T. Gough, R. Vafabakhsh, and R. Golestanian, Self-Motile Colloidal Particles: From Directed Propulsion to Random Walk, Phys. Rev. Lett. **99**, 048102 (2007).

[6] R. Golestanian, T. B. Liverpool, and A. Ajdari, Propulsion of a Molecular Machine by Asymmetric Distribution of Reaction Products, Phys. Rev. Lett. **94**, 220801 (2005).

[7] K. Yamamoto, R. M. Macnab, and Y. Imae, Repellent response functions of the TRG and TAP chemoreceptors of *Escherichia coli*, J. Bacteriol. **172**, 383 (1990).

[8] G. Rosen, Fundamental theoretical aspects of bacterial chemotaxis, J. Theor. Biol. **41**, 201 (1973).

[9] V. Sourjik, Receptor clustering and signal processing in *e. coli* chemotaxis, Trends Microbiol. **12**, 569 (2004).

[10] J. L. Fitzpatrick, C. Willis, A. Devigili, A. Young, M. Carroll, H. R. Hunter, and D. R. Brison, Chemical signals from Eggs facilitate cryptic female choice in humans, Proc. R. Soc. B **287**, 20200805 (2020).
[11] P. J. Krug, J. A. Riffell, and R. K. Zimmer, Endogenous signaling pathways and chemical communication between sperm and egg, J. Exp. Biol. **212**, 1092 (2009).
[12] M. C. Marchetti, J. F. Joanny, T. B. Liverpool S. Ramaswamy, Madan Rao J. Prost, and R. Aditi Simha, Hydrodynamics of soft active matter, Rev. Mod. Phys. **85**, 1143 (2013).
[13] C. Bechinger, R. Di Leonardo, H. Löwen, C. Reichhardt, G. Volpe, and G. Volpe, Active particles in complex and crowded environments, Rev. Mod. Phys. **88**, 045006 (2016).
[14] B. V. Derjaguin, G. Sidorenkov, E. Zubashchenko, and E. Kiseleva, Kinetic phenomena in the boundary layers of liquids, I. The capillary osmosis, Prog. Surf. Sci. **43**, 138 (1993).
[15] J. L. Anderson, M. E. Lowell, and D. C. Prieve, Motion of a particle generated by chemical gradients, Part 1. Non-electrolytes, J. Fluid Mech. **117**, 107 (1982).
[16] J. Burdick, R. Laocharoensuk, P. M. Wheat, J. D. Posner, and J. Wang, Synthetic nanomotors in microchannel networks: Directional microchip motion and controlled manipulation of cargo, J. Am. Chem. Soc. **130**, 8164 (2008).
[17] G. A. Ozin, I. Manners, S. Fournier-Bidoz, and A. Arsenault, Dream nanomachines, Adv. Mater. **17**, 3011 (2005).
[18] R. Golestanian, T. B. Liverpool, and A. Ajdari, Designing phoretic micro- and nano-swimmers, New J. Phys. **9**, 126 (2007).
[19] S. Michelin and E. Lauga, Phoretic self-propulsion at finite Péclet numbers, J. Fluid Mech. **747**, 572 (2014).
[20] G. Natale, C. Datt, S. G. Hatzikiriakos, and G. J. Elfring, Autophoretic locomotion in weakly viscoelastic fluids at finite Péclet number, Phys. Fluids **29** (12), 123102 (2017).
[21] H. J. Keh and J. C. Weng, Diffusiophoresis of colloidal spheres in nonelectrolyte gradients at small but finite Péclet number, Colloid Polym. Sci. **279**, 305 (2001).
[22] R. S. Subramanian, Slow migration of a gas bubble in a thermal gradient, AIChE J. **27**, 646 (1981).
[23] A. M. Leshansky, O. M. Lavrenteva, and A. Nir, Thermocapillary migration of bubbles: Convective effects at low Péclet number, J. Fluid Mech. **443**, 377 (2001).
[24] A. S. Khair, Diffusiophoresis of colloidal particles in neutral solute gradients at finite Péclet number, J. Fluid Mech. **731**, 64 (2013).
[25] M. N. Popescu, W. E. Uspal, C. Bechinger, and P. Fischer, Chemotaxis of active Janus nanoparticles, Nano Lett. **18**, 5345 (2018).
[26] M. Tătulea-Codrean and E. Lauga, Artificial chemotaxis of phoretic swimmers: Instantaneous and long-time behaviour, J. Fluid Mech. **856**, 921 (2018).
[27] P. M. Vinze, A. Choudhary, and S. Pushpavanam, Motion of an active particle in a linear concentration gradient, Phys. Fluids **33**, 032011 (2021).
[28] M. Van Dyke, *Perturbation Methods in Fluid Mechanics*, *Applied Mathematics and Mechanics Vol. 8* (Academic Press, New York, 1965).
[29] H. A. Stone and A. D. T. Samuel, Propulsion of Microorganisms by Surface Distortions, Phys. Rev. Lett. **77**, 4102 (1996).
[30] A. E. Frankel and A. S. Khair, Dynamics of a self-diffusiophoretic particle in shear flow, Phys. Rev. E **90**, 013030 (2014).
[31] L. G. Leal, *Advanced Transport Phenomena: Fluid Mechanics and Convective Transport Process*, Cambridge Series in Chemical Engineering (Cambridge University Press, Cambridge, UK, 2007) .
[32] M. Abramowitz and I. Stegun, *Pocketbook of Mathematical Functions—Abridged Edition of Handbook of Mathematical Functions* (Verlag Harri Deutsch, Frankfurt am Main, Germany, 1984).
[33] Y. Fily and M. C. Marchetti, Athermal Phase Separation of Self-Propelled Particles with No Alignment, Phys. Rev. Lett. **108**, 235702 (2012).
[34] A. Zöttl and H. Stark, Emergent behavior in active colloids, J. Phys.: Condens. Matter **28**, 253001 (2016).
[35] T. Traverso and S. Michelin, Hydrochemical interactions in dilute phoretic suspensions: From individual particle properties to collective organization, Phys. Rev. Fluids **5**, 104203 (2020).